WORLD JOURNAL OF PHARMACEUTICAL RESEARCH
Coden USA: WJPRAP Impact Factor 8.453
Volume 14, Issue 19, 1257-1275. Research Article ISSN 2277–7105

EFFECT OF COBALT DOPING ON THE STRUCTURAL, OPTICAL, AND PHOTOCATALYTIC PROPERTIES OF ZNO FOR METHYLENE BLUE DEGRADATION

***Rajendra K. Pawar**

*Department of Chemistry, Mahatma Gandhi Vidyamandir's Maharaja Sayajirao Gaikwad Arts, Science and Commerce College (Affiliated to Savitribai Phule Pune University, Pune), Malegaon, Nashik - 423105, India.

Article Received on 06 Sept. 2025,
Article Revised on 26 Sept. 2025,
Article Published on 01 Oct. 2025,

https://doi.org/10.5281/zenodo.17292427

***Corresponding Author**

Rajendra K. Pawar

Department of Chemistry, Mahatma Gandhi Vidyamandir's Maharaja Sayajirao Gaikwad Arts, Science and Commerce College (Affiliated to Savitribai Phule Pune University, Pune), Malegaon, Nashik - 423105, India.

How to cite this Article: *Rajendra K. Pawar. (2025). Effect Of Cobalt Doping On The Structural, Optical, And Photocatalytic Properties Of Zno For Methylene Blue Degradation. World Journal of Pharmaceutical Research, 14(19), 1257–1275.

ABSTRACT

The uncontrolled discharge of synthetic dyes into aquatic environments poses a significant environmental and health hazard, with methylene blue (MB) being one of the most persistent pollutants. In this study, pure zinc oxide (ZnO) and cobalt-doped ZnO (Co–ZnO1 and Co–ZnO2) nanoparticles were synthesized via a co-precipitation method to evaluate the effect of cobalt incorporation on structural, optical, morphological, and photocatalytic properties. X-ray diffraction (XRD) confirmed the presence of ZnO and cobalt oxide phases with average crystallite sizes of 35.72 nm (ZnO), 36.22 nm (Co–ZnO1), and 45.27 nm (Co–ZnO2). UV–Vis absorption spectra revealed bandgap modifications, with Co doping inducing blue shifts and bandgap broadening (Eg = 3.28 eV for ZnO, 3.96 eV for Co–ZnO1, and 3.47 eV for Co–ZnO2). FT-IR analysis validated Zn–O lattice vibrations and Co incorporation, while FE-SEM and EDS confirmed morphology changes and successful cobalt substitution. Photocatalyti studies demonstrated efficient degradation of MB under visible-light irradiation, with maximum performance observed for undoped ZnO (86.33% degradation at 140 min), followed by Co–ZnO2 (76.22%) and Co–ZnO1 (66.11%). The reduced performance of doped samples was attributed to dopant-induced aggregation, charge recombination, and surface morphology alterations, although Co–ZnO2 retained moderate

activity due to an improved balance between dopant level and bandgap tuning. These findings highlight the complex interplay between dopant concentration, crystallite size, and surface morphology in tailoring ZnO-based photocatalysts for dye degradation.

KEYWORDS: Zinc oxide; Cobalt doping; Photocatalysis; Methylene blue degradation; Co-precipitation.

GRAPHICAL ABSTRACT

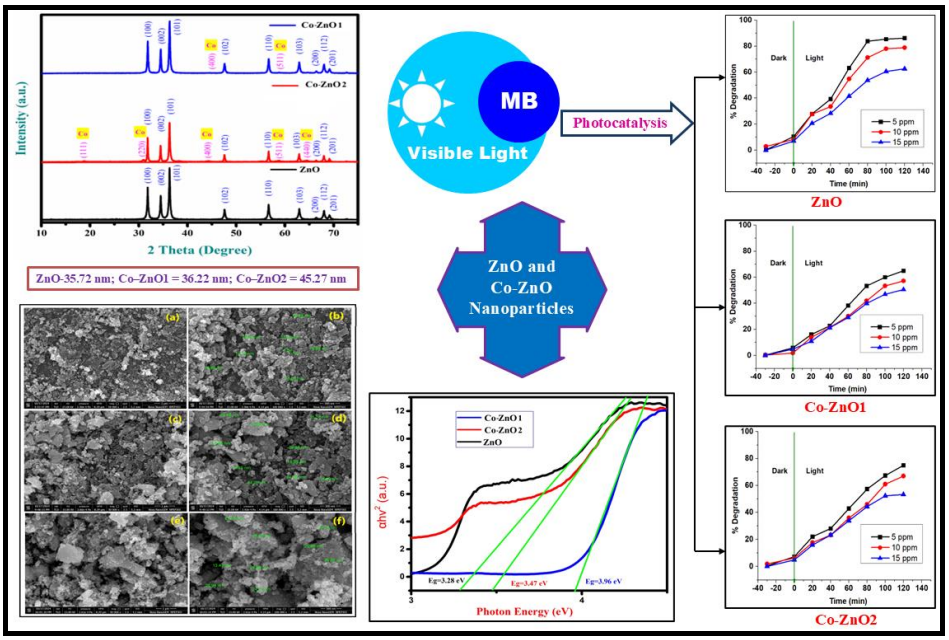

1. INTRODUCTION

The rapid expansion of industrialization and urbanization has resulted in the discharge of large quantities of synthetic dyes into aquatic systems, posing a serious threat to the environment and human health.[1-3] Among these dyes, methylene blue (MB), a cationic thiazine dye widely used in textile, printing, and paper industries, is particularly persistent and toxic due to its complex aromatic structure, low biodegradability, and potential carcinogenic effects.[4-6] Therefore, the development of efficient, sustainable, and cost-effective methods for MB degradation is of great importance.[7-9] Semiconductor-based photocatalysis has emerged as a promising green technology for the degradation of organic pollutants under solar or artificial light irradiation.[10, 11] Zinc oxide (ZnO), a wide bandgap semiconductor, has attracted significant attention due to its excellent optical absorption, high exciton binding energy, non-toxicity, chemical stability, and low cost.[12,13]

Various strategies such as morphological control, surface modification, and heteroatom doping have been explored for tuning the physical and chemical properties of the nanomaterials.[14-16] Among them, transition-metal ion doping has been considered an effective approach to tailor the electronic structure, reduce the bandgap, suppress charge carrier recombination, and enhance the visible-light photocatalytic activity of ZnO.[16] In recent years, several studies have reported the synthesis of Co-doped ZnO nanostructures with altered physical and chemical properties.[17-20] However, the relationship between the structural modifications induced by Co incorporation, the resulting changes in optical behaviour, and their correlation with photocatalytic activity toward MB degradation remains to be systematically investigated.

In this work, I report the synthesis of Co-doped ZnO nanomaterials and systematically study the effect of Co incorporation on their structural, optical, and photocatalytic properties. X-ray diffraction (XRD), Fourier-transform infrared spectroscopy (FTIR), UV–Vis absorption spectroscopy, FE-SEM and EDS analysis were employed to investigate the structural, optical and chemical modifications. The photocatalytic activity of the prepared samples was evaluated using methylene blue as a model pollutant under visible-light irradiation. The influence of Co doping on dye degradation efficiency, electron–hole recombination, and possible photocatalytic mechanisms are discussed in detail.

2. MATERIALS AND METHODS

2.1. General remarks

All chemicals used in the present study, including zinc nitrate hexahydrate ($Zn(NO_3)_2 \cdot 6H_2O$), cobalt nitrate hexahydrate ($Co(NO_3)_2 \cdot 6H_2O$), and sodium hydroxide (NaOH), were of analytical grade and used without further purification. Double-distilled water was employed throughout the synthesis process. The Co-doped ZnO samples were prepared by the co-precipitation method using appropriate dopant concentrations to achieve desired levels of cobalt incorporation. All experiments were carried out under identical conditions to maintain reproducibility.

2.2. Synthesis of ZnO and Co-doped ZnO

Zinc oxide (ZnO) nanoparticles and cobalt-doped ZnO samples (Co-ZnO1 and Co-ZnO2) were synthesized by a simple co-precipitation method using zinc nitrate hexahydrate ($Zn(NO_3)_2 \cdot 6H_2O$) and cobalt nitrate hexahydrate ($Co(NO_3)_2 \cdot 6H_2O$) as metal precursors. In a typical procedure, the required amount of zinc nitrate was dissolved in distilled water under

constant stirring, and for the doped samples, an appropriate dopant concentration of cobalt nitrate was added to the solution to obtain Co-ZnO1 and Co-ZnO2, respectively. Sodium hydroxide (NaOH) solution was then added drop wise until the pH of the solution reached alkaline conditions (pH ~10), leading to the formation of a precipitate. The mixture was stirred for a four hours, and the resulting precipitate was filtered, thoroughly washed with distilled water and ethanol to remove impurities, and dried in an oven at 100 °C. The dried product was finally calcined at an appropriate temperature (450 °C) to obtain ZnO, Co-ZnO1, and Co-ZnO2 nanopowders.

3. RESULTS AND DISCUSSION

3.1.X-Ray Diffraction analysis

The X-ray diffraction analysis of undoped ZnO, 5% Co-doped ZnONPs, and 3% Co-doped ZnONPs is depicted in Figure 1 The peak positions observed for pure ZnO nanoparticles corresponded to the JCPDS #36-1451 standard, while those for the 3% Co-doped ZnO NPs and 5% Co-doped ZnONPs matched with JCPDS #36-1451 for ZnO and JCPDS #43-1003 for cobalt oxide. Pure ZnO peaks are denoted in blue brackets, while cobalt oxide peaks are indicated in pink brackets. Peaks at positions 31.824, 34.499, 36.314, 47.601, 56.640, 62.950, 66.431, 68.028, and 69.131 are attributed to pure ZnO NPs, whereas peaks at 18.870, 30.928, 44.277, 58.803, and 64.527 are indicative of cobalt oxide. It is noteworthy that an increase in the percentage of cobalt doping leads to the appearance of additional planes in the XRD spectrum. The XRD analysis confirms the presence of both ZnO and cobalt oxide phases, with no discernible impurities detected. The non-uniform distribution of peak intensities suggests crystalline substances. The preferred crystallographic direction was found to be along the (101) plane, and the similarity in peak positions between the two samples indicates minimal strain introduced during nanoparticle synthesis.

Debye Scherer formula (Eq. 1) was used to calculate crystallite size.[21, 22]

$$D = \frac{0.94\,\lambda}{\beta \cos \theta}(01)$$

The crystallite size was determined using Eq. 1. The average crystallite size for undoped ZnO nanoparticles was calculated to be 35.72 nm. In contrast, the average crystallite size for Co-ZnO2 NPs was found to be 45.27 nm. The average crystallite size for Co-ZnO1 NPs was found to be 36.22 nm.

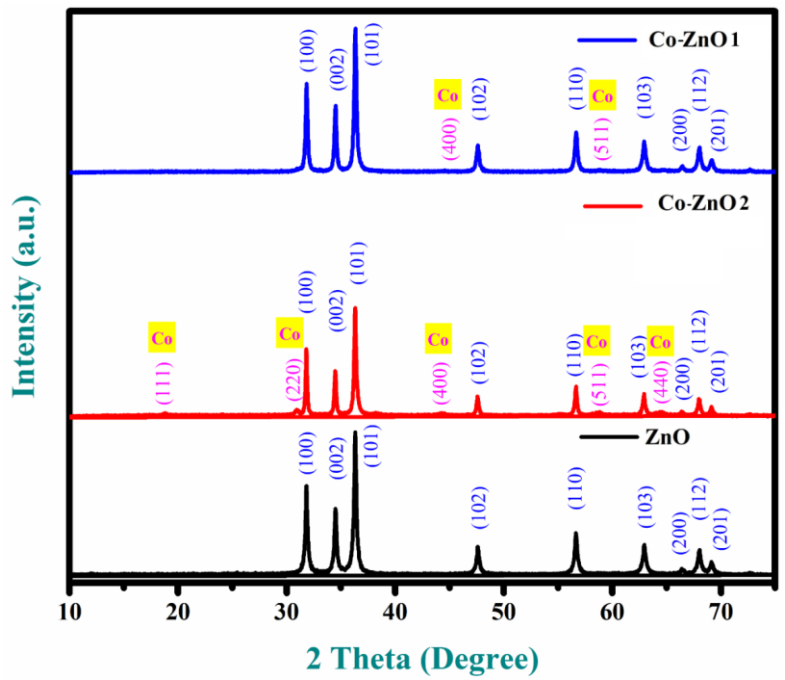

Figure 1: XRD of undoped ZnO, Co-ZnO1, and Co-ZnO2.

3.2. Optical study

The UV–Visible absorption spectra of undoped ZnO and Co-doped ZnO nanomaterials provide crucial insights into the optical properties and electronic structure modifications induced by doping. In general, ZnO is a wide bandgap semiconductor that exhibits a sharp absorption edge in the UV region, primarily due to electronic transitions from the valence band to the conduction band. In the present UV-Vis spectra (Figure 2), the undoped ZnO sample shows two strong absorption bands(around 300 and 370nm), which are consistent with reported data.[23, 24] Upon cobalt incorporation (Co–ZnO1 and Co–ZnO2), the absorption profile undergoes significant changes: the absorption edge shifts slightly towards shorter wavelengths (blue shift). This blue shift indicates a broadening of the optical bandgap, which can be attributed to the substitution of Cointo the ZnO lattice sites. The optical bandgap of ZnO and Co-doped ZnO nanomaterials can be estimated from the Tauc plot data.[23, 24] Undoped ZnO exhibits a direct bandgap transition with an Eg value of 3.28 eV(Figure 3), which is close to the reported intrinsic bandgap of ZnO.[23, 24] Upon cobalt doping, significant changes are observed in the band structure. For the Co–ZnO1 nanomaterial, the absorption edge shifts toward higher energy, giving a wider bandgap of 3.96 eV(Figure 3). On the other hand, the Co–ZnO2 sample shows a slightly reduced bandgap of 3.47 eV as compared to Co–ZnO1 (Figure 3).

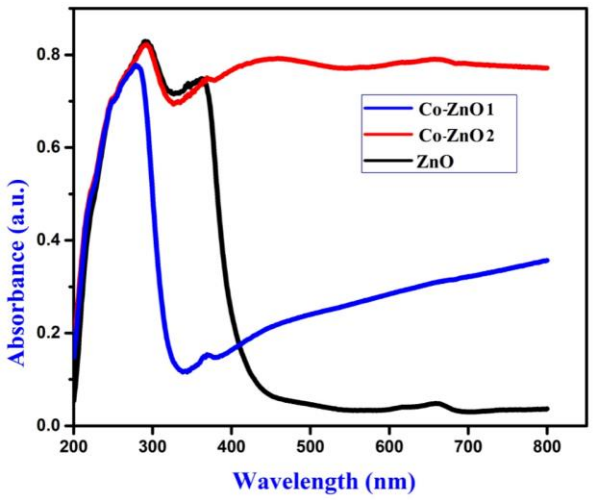

Figure 2: UV-Vis spectra of undoped ZnO, Co-ZnO1, and Co-ZnO2.

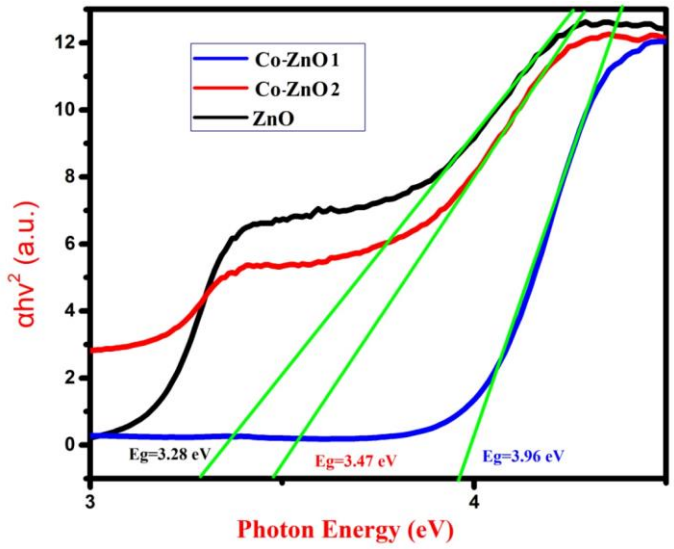

Figure 3: Tauc plot of undoped ZnO, Co-ZnO1, and Co-ZnO2.

3.3. FT-IR Study

The Fourier Transform Infrared (FT-IR) spectra shown in the Figure 4 provide important information about the functional groups and vibrational modes present in undoped ZnO and Co-doped ZnO nanomaterials. FT-IR spectroscopy is widely employed to investigate the bonding environment, lattice vibrations, and surface adsorbed species in metal oxides.[25, 26] The characteristic absorption bands in the low wavenumber region (400–700 cm^{-1}) are typically assigned to metal–oxygen stretching vibrations, which in this case correspond to Zn–O bonds in the ZnO lattice.[27-29] For the undoped ZnO nanomaterial showed absorption band at 443.55 cm^{-1}, which is attributed to the stretching vibrations of Zn–O bonds, confirming the formation of ZnO. In the Co-doped ZnO naomaterials, similar absorption bands are detected at 445.48, and 458.97 cm^{-1}indicating that cobalt substitution does not

disrupt the fundamental Zn–O lattice vibrations, though slight shifts in band positions reflect changes in bond strength and local lattice distortions due to Co incorporation. Additionally, a distinct absorption around 665 cm^{-1} appears in the doped samples, which may correspond to modified Co–O vibrations, further supporting successful cobalt doping.[30] Thus, the FT-IR spectra confirm the structural integrity of ZnO upon cobalt doping, while also highlighting subtle vibrational shifts that reveal the interaction of Co ions within the ZnO lattice.

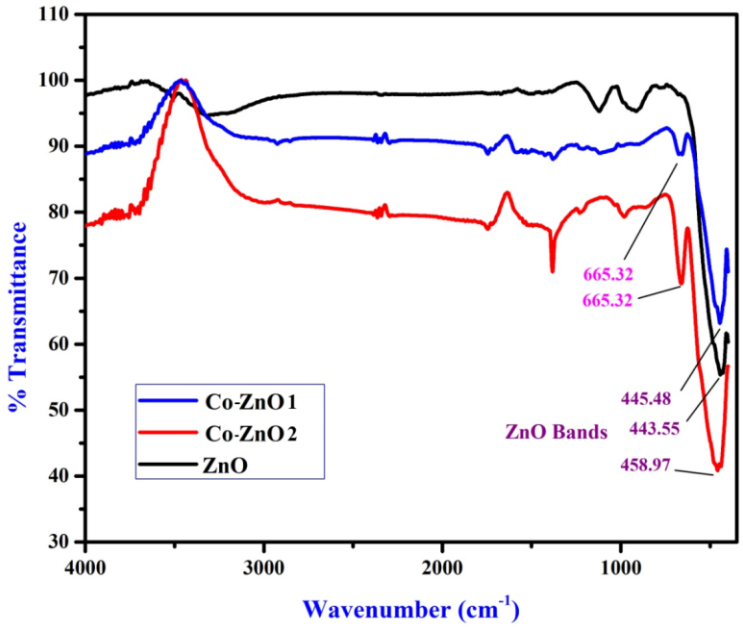

Figure 4: FT-IR spectra of undoped ZnO, Co-ZnO1, and Co-ZnO2.

3.4. FE-SEM and EDS study

The FE-SEM micrographs of undoped and Co-doped ZnO nanoparticles reveal notable morphological variations upon cobalt incorporation. Pure ZnO (Figure 5a-b) exhibits densely packed, nearly spherical nanoparticles with uniform distribution and smooth texture. The average crystallite size estimated from XRD using the Debye–Scherrer equation was 35.72 nm, which is in good agreement with the nanoscale features observed in FE-SEM. These uniform, well-dispersed nanostructures provide a high surface-to-volume ratio, which can explain the superior photocatalytic performance of pristine ZnO. For Co-ZnO1 (Figure 5c-d) the surface morphology becomes more irregular, with smaller aggregates dispersed over the matrix. Although the crystallite size remains comparable **(**36.22 nm), the increased surface roughness and local aggregation may reduce the number of accessible active sites, which is consistent with its comparatively lower photocatalytic activity. In contrast, Co-ZnO2 (Figure 5e-f) shows a drastic morphological transformation, with larger, irregular, and aggregated

nanoparticles forming heterogeneous clusters. The average crystallite size increases significantly to 45.27 nm, indicating Co-induced lattice strain and crystallite growth. Despite the increase in particle size and agglomeration, the modified surface morphology and possible defect states introduced by higher Co doping appear to enhance light absorption and charge carrier separation, resulting in improved photocatalytic activity compared to Co-ZnO1, though still lower than pure ZnO. The FE-SEM analysis coupled with crystallite size data provided strong evidence that the balance between particle size, morphology, and surface defects played a crucial role in determining photocatalytic efficiency, explaining the observed activity trend of ZnO > Co-ZnO2 > Co-ZnO1**.**

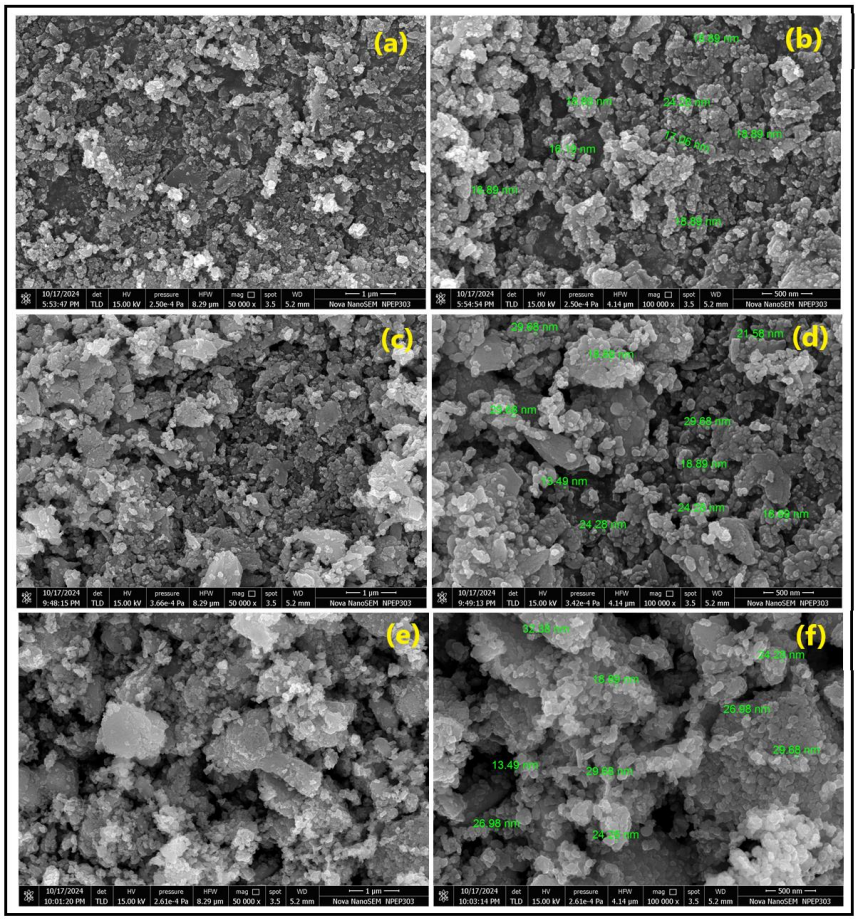

Figure 5: FE-SEMImages of undoped ZnO, Co-ZnO1, and Co-ZnO2.

The elemental composition of ZnO and Co-doped ZnO nanoparticles was analyzed by energy dispersive X-ray spectroscopy (EDS), as shown in (Figure 6a-c) (Figure 6a-ZnO, Figure 6b-Co-ZnO1, Figure 6c-Co-ZnO2). The EDS spectrum of pure ZnO confirmed the presence of only Zn and O peaks, with no impurity signals, indicating high purity of the synthesized nanoparticles. The atomic percentages of Zn and O were found to be 47.64% and 52.36%,

respectively, which is close to the stoichiometric ratio, confirming the formation of ZnO. In the case of Co-ZnO1, additional peaks corresponding to Co were observed alongside Zn and O, confirming successful doping of Co into the ZnO lattice. The Co content was estimated to be ~2.15 wt% (2.06 at.%), suggesting a relatively low substitution level. For Co-ZnO2, the Co peaks were more prominent, with the elemental composition showing ~9.90 wt% (8.08 at.%) Co, which is significantly higher compared to Co-ZnO1. This indicates that higher doping concentrations were successfully achieved in the Co-ZnO2 sample. The progressive increase in Co signal intensity across the spectra strongly confirms effective incorporation of cobalt ions into the ZnO matrix without the appearance of any secondary impurity peaks, demonstrating that the synthesis method yields phase-pure doped nanoparticles. Furthermore, the variation in elemental composition correlates with the observed FE-SEM morphologies and crystallite sizes, where higher Co content in Co-ZnO2 led to larger particle size and agglomeration, while the lower Co content in Co-ZnO1 maintained a finer morphology. These compositional findings also support the photocatalytic activity results, where pure ZnO exhibited the highest activity, followed by Co-ZnO2 and then Co-ZnO1, suggesting that the interplay of Co concentration, particle morphology, and crystallite size strongly influences photocatalytic efficiency. Figure 7 represents the elemental mapping images of undoped ZnO, Co-ZnO1, and Co-ZnO2 showing the uniform distribution of Zn and O in pure ZnO, along with the successful incorporation and homogeneous dispersion of Co in the doped samples without any detectable impurities.

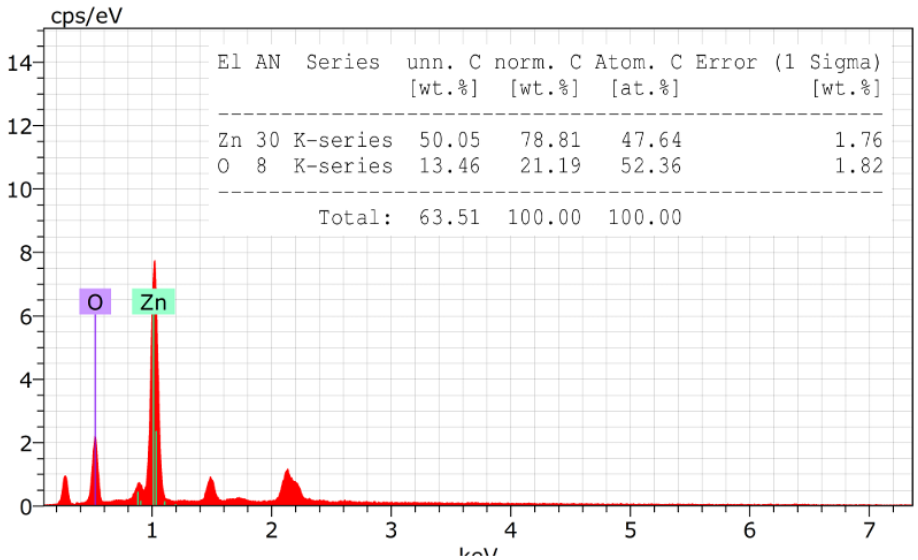

Figure 6a: EDSgraph of undoped ZnO.

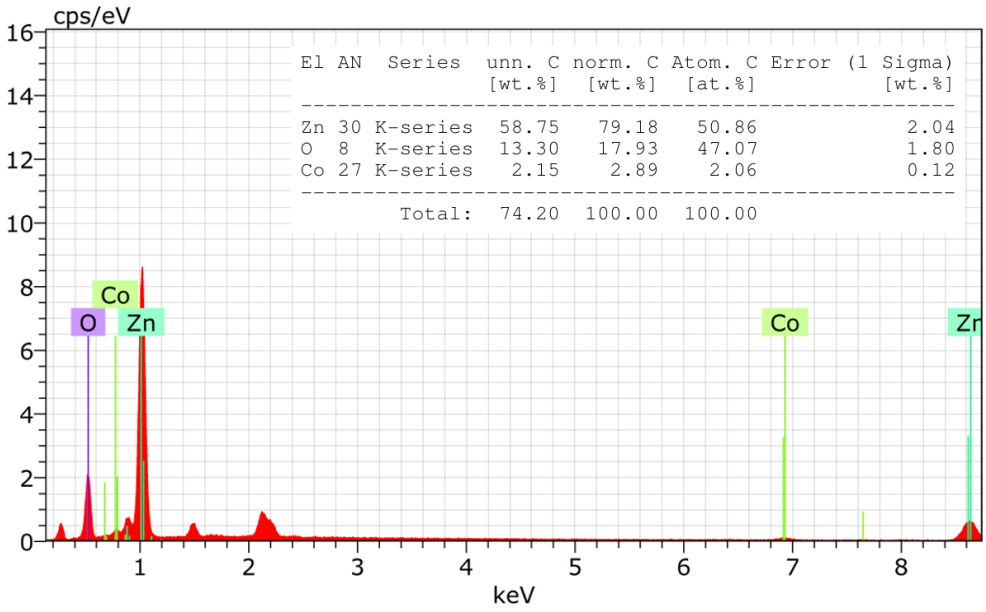

Figure 6b: EDS graph of Co-ZnO1.

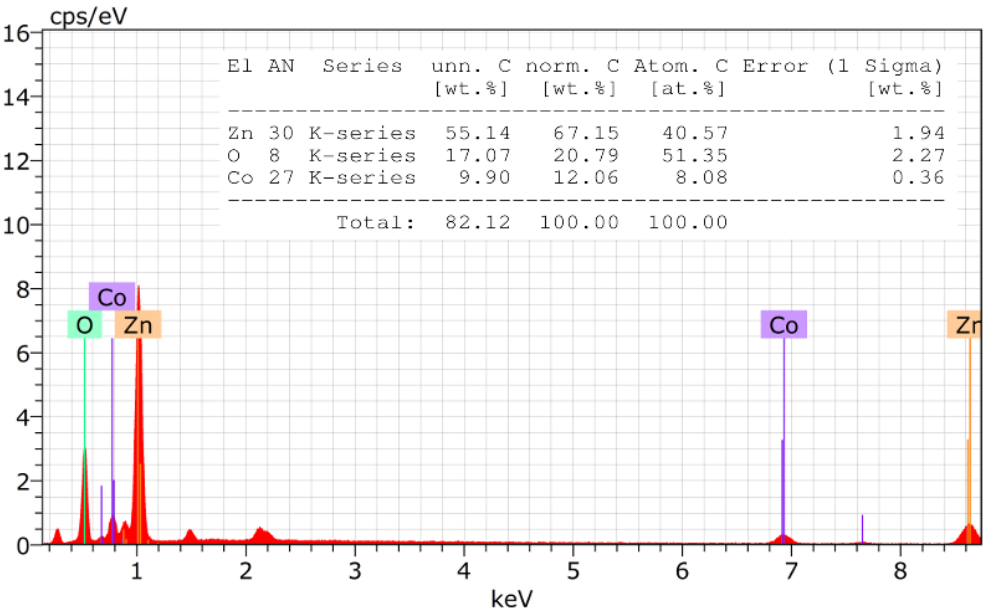

Figure 6c: EDS graph of Co-ZnO2.

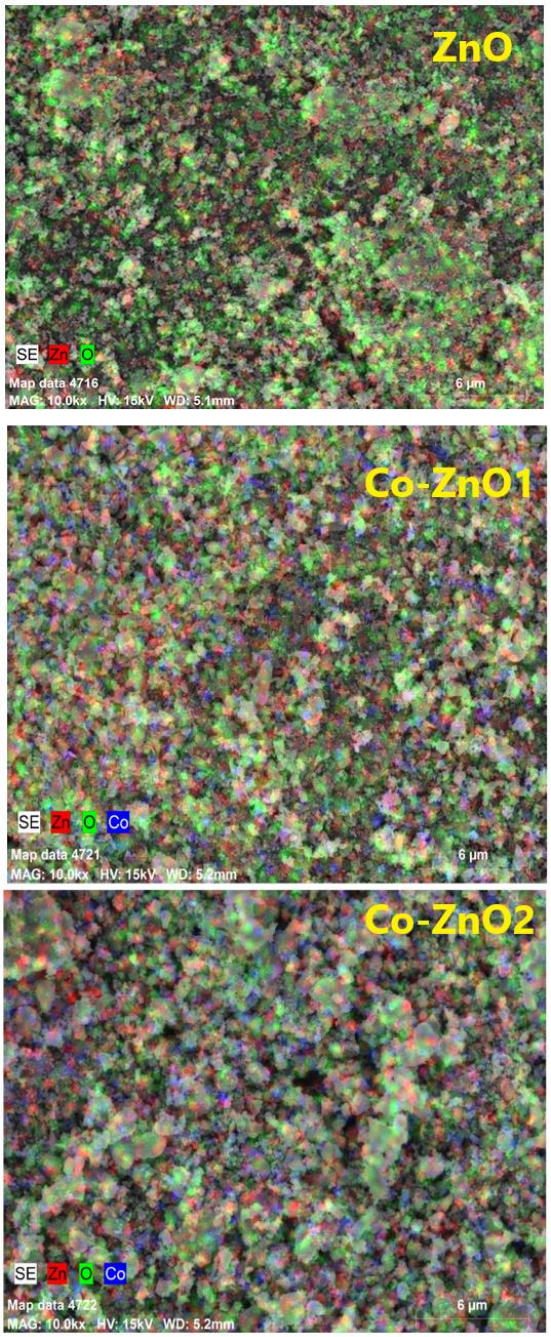

Figure 7: Elemental mapping images of undoped ZnO, Co-ZnO1, and Co-ZnO2.

3.5. Photocatalysis study

The catalyst dose optimization study of undoped ZnO for MB dye degradation demonstrated that increasing the ZnO loading enhances the photocatalytic activity up to a certain limit. Figure 8 depicts the Catalyst dose optimization for photocatalytic degradation, showing the effect of varying catalyst concentrations of ZnO on the degradation efficiency. At lower catalyst loading (0.2 g/L), the degradation efficiency remained modest, reaching only 47.04% after 60 min. A higher dose of 0.4 g/L significantly improved the performance (64.33% at 60

min), while 0.6 g/L shows the maximum efficiency (67.45% at 60 min). The improvement with increasing ZnO dose is attributed to the greater availability of active sites and photon absorption, which generates more reactive species for dye degradation. However, the marginal gain from 0.4 g/L to 0.6 g/L suggested that beyond the optimum level, excess catalyst may cause light scattering and shielding effects, reducing photocatalytic efficiency. Thus, 0.4 g/L appeared to be the optimal range for efficient degradation.

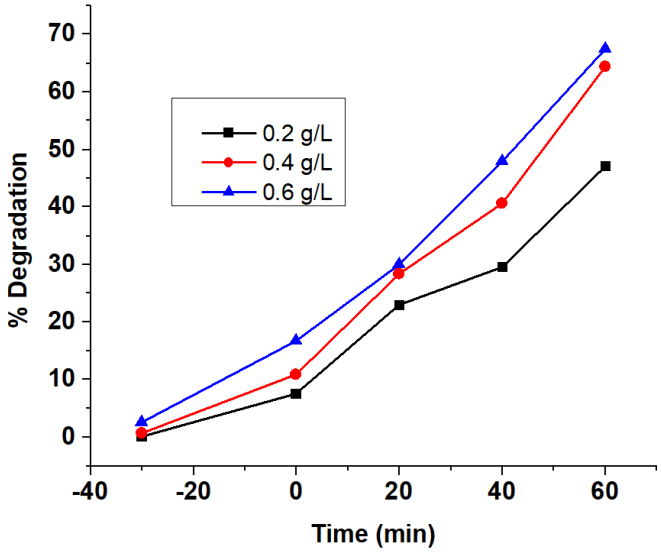

Figure 8: Catalyst dose optimization.

The effect of initial MB concentration (5, 10, and 15 ppm) on the photocatalytic degradation efficiency was investigated using undoped ZnO, Co–ZnO1, and Co–ZnO2. Figure 8a–cillustrate the effect of initial dye concentration on the photocatalytic degradation efficiency of ZnO, Co-ZnO1, and Co-ZnO2 nanomaterials. In all three cases, a common trend was observed: lower dye concentrations favoured higher degradation efficiency, while increasing concentration reduced photocatalytic performance. For undoped ZnO, the highest degradation (~86.14% at 120 min) was achieved at 5 ppm, which decreased to 78.75% and 62.56% for 10 and 15 ppm, respectively. A similar trend was seen for Co–ZnO1, with degradation efficiencies of 65.03%, 57.14%, and 50.58% at 5, 10, and 15 ppm, respectively. Co–ZnO2 showed slightly better performance than Co–ZnO 1, achieving 75.01% at 5 ppm, 66.98% at 10 ppm, and 53.34% at 15 ppm. The decline in efficiency at higher dye concentrations is attributed to light attenuation, competitive adsorption of dye molecules, and partial blocking of catalyst active sites, which reduces the generation of reactive oxygen species. Among the catalysts, ZnO showed the highest overall degradation efficiency, while Co–ZnO2 outperformed Co–ZnO1 due to its better balance of dopant incorporation, which improved

visible-light activity without introducing excessive charge recombination centers. Thus, 5 ppm is the optimal dye concentration for maximum degradation, and catalyst efficiency follows the order: ZnO > Co–ZnO2 > Co–ZnO1.

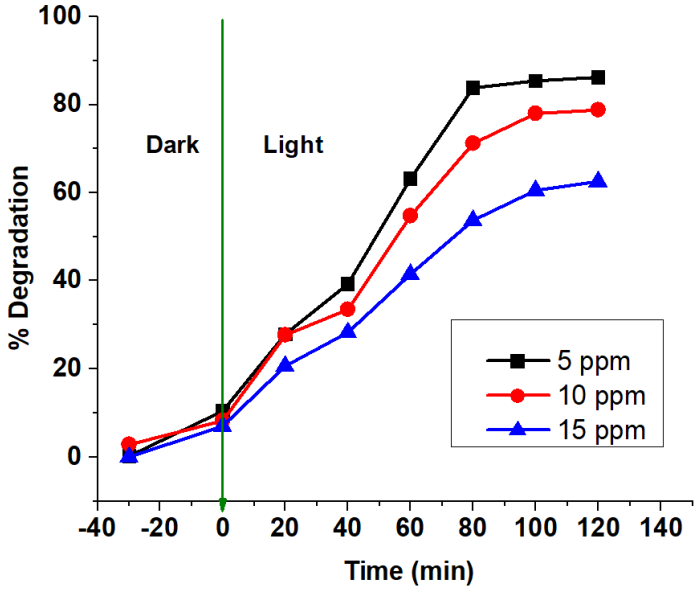

Figure 8a: Effect of initial dye concentration for ZnO nanomaterial.

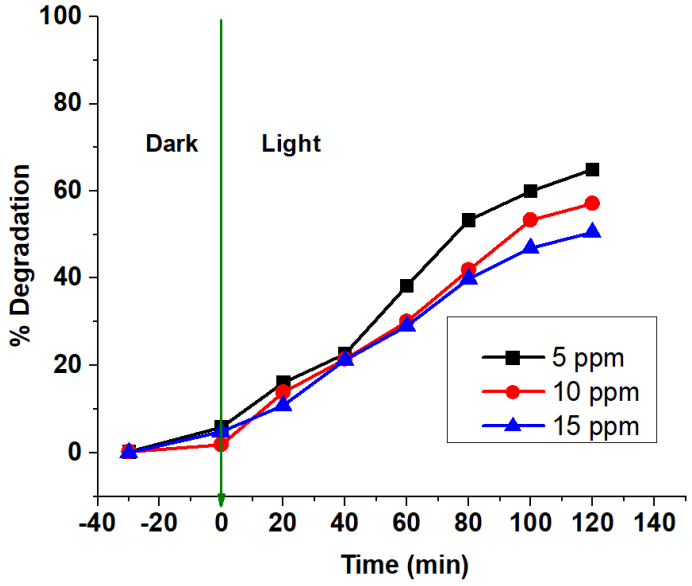

Figure 8b: Effect of initial dye concentration for Co-ZnO1 nanomaterial.

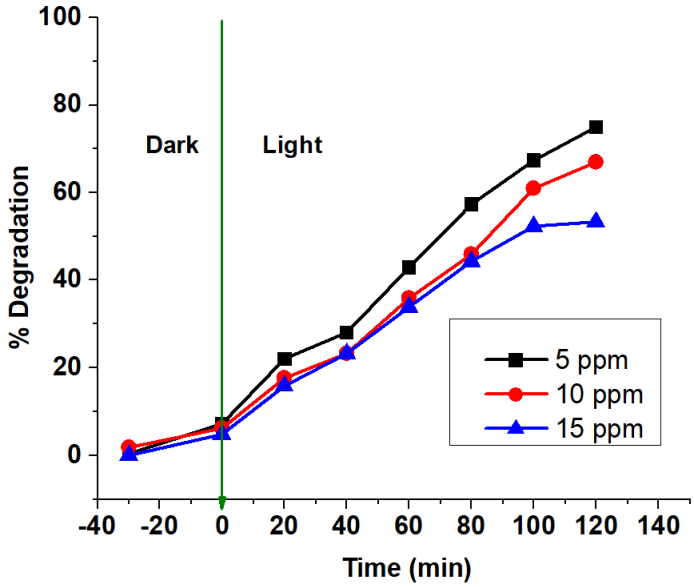

Figure 8c: Effect of initial dye concentration for Co-ZnO2 nanomaterial.

Figure 9 shows the effect of contact time on the photocatalytic degradation of methylene blue (MB) dye using undoped ZnO, Co-ZnO1, and Co-ZnO2 nanomaterials. The contact time study for the photocatalytic degradation of MB dye using ZnO and Co-doped ZnO catalysts revealed a time-dependent increase in degradation efficiency. Initially, at 0 min, all catalysts show rapid adsorption of dye molecules, with ZnO (10.36%) slightly outperforming Co–ZnO nanomaterials. However, as reaction time progresses, the catalytic performance diverges. Undoped ZnO exhibits the highest degradation (86.33%) within 140 min, while Co–ZnO2 (76.22%) and Co–ZnO1 (66.11%) showed comparatively lower efficiencies. The results indicated that although Co doping declines the photocatalytic activity compared to undoped ZnO.

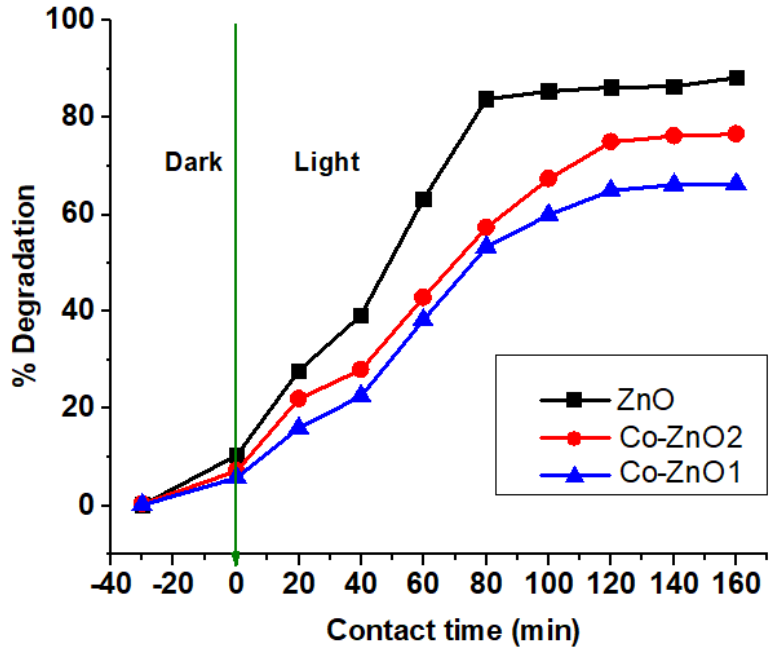

Figure 9: Effect of contact time for degradation of MB dye using undoped ZnO, Co-ZnO1, and Co-ZnO2.

CONCLUSION

This study systematically investigated the effect of cobalt incorporation on the structural, optical, and photocatalytic properties of ZnO nanoparticles synthesized via co-precipitation. XRD, FT-IR, UV–Vis, FE-SEM, and EDS analyses confirmed successful cobalt doping and corresponding modifications in crystallite size, morphology, and band structure. Photocatalytic degradation studies revealed that pure ZnO exhibited the highest efficiency toward methylene blue degradation, followed by Co–ZnO2 and Co–ZnO1. The decline in photocatalytic performance of doped samples was attributed to particle agglomeration and recombination centers introduced by cobalt incorporation, despite favorable bandgap shifts. These results suggest that controlled doping levels are essential to optimize the trade-off between improved light absorption and minimized charge recombination. Overall, undoped ZnO remains superior for MB degradation, but optimized Co-doped ZnO can serve as a promising candidate for visible-light-driven photocatalytic applications.

Funding

The author did not receive any specific grant from funding agencies in the public, commercial, or not-for-profit sectors for this research work.

Conflicts of Interest / Competing Interests

The author declares no conflict of interest regarding the publication of this article.

Ethical Approval

This research does not involve human participants or animals; hence, ethical approval is not required.

Consent to Participate

Not applicable.

Consent for Publication

The author gives full consent for the publication of this manuscript in the journal.

Availability of Data and Materials

All data generated or analyzed during this study are included in the manuscript. Additional datasets are available from the corresponding author upon reasonable request.

Authors' Contributions

Rajendra K. Pawar: Conceptualization, Methodology, Investigation, Data curation, Formal analysis, Writing – original draft, Review & editing.

ACKNOWLEDGMENTS

The author gratefully acknowledges the Department of Chemistry, Mahatma Gandhi Vidyamandir's Maharaja Sayajirao Gaikwad Arts, Science and Commerce College, Malegaon, for providing laboratory facilities and necessary support to carry out this research work. The author is grateful to SPPU, Pune for providing spectral analysis of the nanomaterials.

REFERENCES

1. Saxena, V., Water quality, air pollution, and climate change: investigating the environmental impacts of industrialization and urbanization. *Water, Air, & Soil Pollution*, 2025; *236*(2): 73.
2. Islam, T., Repon, M.R., Islam, T., Sarwar, Z. and Rahman, M.M., Impact of textile dyes on health and ecosystem: a review of structure, causes, and potential solutions. *Environmental Science and Pollution Research*, 2023; *30*(4): 9207-9242.

3. Kolya, H. and Kang, C.W., Toxicity of metal oxides, dyes, and dissolved organic matter in water: implications for the environment and human health. *Toxics*, 2024; *12*(2): 111.
4. Khan, I., Saeed, K., Zekker, I., Zhang, B., Hendi, A.H., Ahmad, A., Ahmad, S., Zada, N., Ahmad, H., Shah, L.A. and Shah, T., Review on methylene blue: its properties, uses, toxicity and photodegradation. *Water*, 2022; *14*(2): 242.
5. Moorthy, A.K., Rathi, B.G., Shukla, S.P., Kumar, K. and Bharti, V.S., Acute toxicity of textile dye Methylene blue on growth and metabolism of selected freshwater microalgae. *Environmental Toxicology and Pharmacology*, 2021; *82*: 103552.
6. Ismail, M., Akhtar, K., Khan, M.I., Kamal, T., Khan, M.A., M Asiri, A., Seo, J. and Khan, S.B., Pollution, toxicity and carcinogenicity of organic dyes and their catalytic bio-remediation. *Current pharmaceutical design*, 2019; *25*(34): 3645-3663.
7. Hamad, H. N. and Idrus, S., Recent developments in the application of bio-waste-derived adsorbents for the removal of methylene blue from wastewater: a review. *Polymers*, 2022; *14*(4): 783.
8. Liu, M., You, X., Li, Y. and Yang, Y., Critical review on development of methylene blue degradation by wet catalytic methods. *Reviews in Chemical Engineering*, 2025; *41*(2): 179-195.
9. Ruan, W., Hu, J., Qi, J., Hou, Y., Zhou, C. and Wei, X., Removal of dyes from wastewater by nanomaterials: a review. *Adv Mater Lett.*, 2019; *10*(1): 9-20.
10. Opoku, F., Govender, K.K., van Sittert, C.G.C.E. and Govender, P.P., Recent progress in the development of semiconductor-based photocatalyst materials for applications in photocatalytic water splitting and degradation of pollutants. *Advanced Sustainable Systems*, 2017; *1*(7): 1700006.
11. Mishra, K., Devi, N., Siwal, S.S., Gupta, V.K. and Thakur, V.K., Hybrid semiconductor photocatalyst nanomaterials for energy and environmental applications: fundamentals, designing, and prospects. *Advanced Sustainable Systems*, 2023; *7*(8): 2300095.
12. Raha, S. and Ahmaruzzaman, M., ZnO nanostructured materials and their potential applications: progress, challenges and perspectives. *Nanoscale advances*, 2022; *4*(8): 1868-1925.
13. Baig, A., Siddique, M. and Panchal, S., A review of visible-light-active zinc oxide photocatalysts for environmental application. *Catalysts*, 2025; *15*(2): 100.
14. Sathyan, B. and Cyriac, J., Functionalization and Surface Modification of Nanomaterials for Electronic and Optoelectronic Device Applications. *Functionalized Nanomaterials for*

Electronic and Optoelectronic Devices: Design, Fabrications and Applications, 2025; 65-99.

15. Medhi, R., Marquez, M.D. and Lee, T.R., Visible-light-active doped metal oxide nanoparticles: review of their synthesis, properties, and applications. *ACS Applied Nano Materials*, 2020; *3*(7): 6156-6185.
16. Waghchaure, R.H., Adole, V.A. and Jagdale, B.S., Photocatalytic degradation of methylene blue, rhodamine B, methyl orange and Eriochrome black T dyes by modified ZnO nanocatalysts: A concise review. *Inorganic Chemistry Communications*, 2022; *143*: 109764.
17. Djerdj, I., Jagličić, Z., Arčon, D. and Niederberger, M., Co-doped ZnO nanoparticles: minireview. *Nanoscale*, 2010; *2*(7): 1096-1104.
18. Šutka, A., Kaeaembre, T., Paerna, R., Juhnevica, I., Maiorov, M., Joost, U. and Kisand, V., 2016. Co doped ZnO nanowires as visible light photocatalysts. *Solid State Sciences*, 2010; *56*: 54-62.
19. Guler, A., Synthesis, Structure, and Magnetic Properties of (Co/Eu) Co-Doped ZnO Nanoparticles. *Coatings*, 2025; *15*(8): 884.
20. Yakushova, N.D., Gubich, I.A., Karmanov, A.A., Komolov, A.S., Koroleva, A.V., Korotcenkov, G. and Pronin, I.A., Photocatalytic Degradation of Toxic Dyes on Cu and Al Co-Doped ZnO Nanostructured Films: A Comparative Study. *Technologies*, 2025; *13*(7): 277.
21. Mustapha, S., Ndamitso, M.M., Abdulkareem, A.S., Tijani, J.O., Shuaib, D.T., Mohammed, A.K. and Sumaila, A., Comparative study of crystallite size using Williamson-Hall and Debye-Scherrer plots for ZnO nanoparticles. *Advances in Natural Sciences: Nanoscience and Nanotechnology*, 2019; *10*(4): 045013.
22. Shinde, R.S., Khairnar, S.D., Patil, M.R., Adole, V.A., Koli, P.B., Deshmane, V.V., Halwar, D.K., Shinde, R.A., Pawar, T.B., Jagdale, B.S. and Patil, A.V., Synthesis and characterization of ZnO/CuO nanocomposites as an effective photocatalyst and gas sensor for environmental remediation. *Journal of Inorganic and Organometallic Polymers and Materials*, 2022; *32*(3): 1045-1066.
23. Waghchaure, R.H., Adole, V.A., Kushare, S.S., Shinde, R.A. and Jagdale, B.S., Visible light prompted and modified ZnO catalyzed rapid and efficient removal of hazardous crystal violet dye from aqueous solution: a systematic experimental study. *Results in Chemistry*, 2023; *5*: 100773.

24. Shaikh, A.A., Patil, M.R., Jagdale, B.S. and Adole, V.A., Synthesis and characterization of Ag doped ZnO nanomaterial as an effective photocatalyst for photocatalytic degradation of Eriochrome Black T dye and antimicrobial agent. *Inorganic Chemistry Communications*, 2023; *151*: 110570.
25. Srinivasan, M.P. and Punithavelan, N., Structural, morphological and dielectric investigations on NiO/CuO/ZnO combined semiconductor metal oxide structures based ternary nanocomposites. *Materials Research Express*, 2018; *5*(7): 075033.
26. Yang, X., Deng, Y., Yang, H., Liao, Y., Cheng, X., Zou, Y., Wu, L. and Deng, Y., Functionalization of mesoporous semiconductor metal oxides for gas sensing: Recent advances and emerging challenges. *Advanced Science*, 2023; *10*(1): 2204810.
27. Lage, V.M., Rodríguez-Fernández, C., Vieira, F.S., da Silva, R.T., Bernardi, M.I.B., de Lima Jr, M.M., Cantarero, A. and de Carvalho, H.B., On the vibrational properties of transition metal doped ZnO: Surface, defect, and bandgap engineering. *Acta Materialia*, 2023; *259*: 119258.
28. Raja, K., Ramesh, P.S. and Geetha, D., Structural, FTIR and photoluminescence studies of Fe doped ZnO nanopowder by co-precipitation method. *Spectrochimica acta part A: molecular and biomolecular spectroscopy*, 2014; *131*: 183-188.
29. Shaikh, A.A., Patil, M.R., Jagdale, B.S. and Adole, V.A., Synthesis and characterization of Ag doped ZnO nanomaterial as an effective photocatalyst for photocatalytic degradation of Eriochrome Black T dye and antimicrobial agent. *Inorganic Chemistry Communications*, 2023; *151*: 110570.
30. Din, M.I., Khalid, R., Hussain, Z., Gul, S. and Mujahid, A., Synthesis and characterization of cobalt doped zinc oxide nanoparticles and their application for catalytic reduction of methylene blue dye. *Desalination and Water Treatment*, 2024; *317*: 100002.